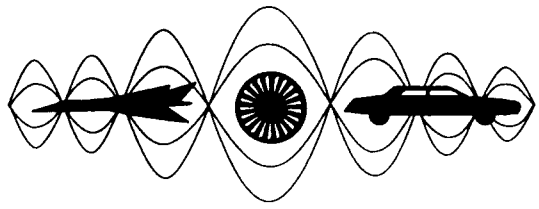

FIFTH INTERNATIONAL CONGRESS ON SOUND AND VIBRATION
DECEMBER 15-18, 1997
ADELAIDE, SOUTH AUSTRALIA

Invited Paper

CONSERVATION OF ENERGY AND MODEL CONVERGENCE USING EXPERIMENTAL SPATIAL POWER FLOW

JONATHAN D. BLOTTER [1] GARY A. FLEMING [2] ROBERT L. WEST [3]

[1] College of Engineering, Idaho State University, Pocatello, ID 83209
[2] NASA Langley Research Center, Hampton, VA 23681-0001
[3] Dept. of Mechanical Engineering, Virginia Polytechnic Institute and State University, Blacksburg, VA, 24061

ABSTRACT

Experimental Spatial Power Flow (ESPF) is a non-intrusive spatially continuous laser based technique for extracting the power flow from vibrating structures. The ESPF approach retains the spatial representation of the power flow, obtained from analytical models, and represents the actual boundary conditions by using experimental data obtained from a scanning laser Doppler Vibrometer. In this paper, ESPF results are compared to the power injected into a simply supported plate which is excited by two shakers placed diagonally across the plate. The two shakers are phased such that one acts as a power source and the other a power sink. The power injected and absorbed by the two shakers is computed from impedance head measurements. Model order convergence capabilities of the power flow computed using the ESPF technique is also demonstrated.

1. INTRODUCTION

Power is defined as the time-averaged product of the generalized forces with the in-phase component of the generalized velocities. The power in a structure can be represented as a vector with both magnitude and direction since the directions of the generalized forces and velocities from which the power is computed are known [1]. When plotting power vectors, a flow type pattern develops and hence the term power flow.

The ESPF method is developed around the high spatial density measurement capability of a scanning laser Doppler vibrometer (SLDV). The spatially dense measurements acquired by the SLDV are used to solve for a spatially continuous 3-D complex-valued representation of

velocity field is integrated in time to obtain the spatially continuous 3-D complex-valued displacement field. From this representation of the displacement field, a complex-valued representation of the generalized forces is obtained. By computing the product of the generalized forces and velocities from these models the power in the structure is obtained. The "best" models of the velocity field and the power flow can be obtained through mesh convergence. Convergence of the velocity-field model is determined by comparing the residuals between the laser data and the velocity solution obtained from the least squares finite element solution. The best converged model is the model in which the residuals are minimized. The best power flow model is determined by the solution which most closely approximates the energy injected into the plate as measured by the impedance heads. As expected, power flow requires a higher model order than the velocity to obtain a converged solution. For a detailed description of the ESPF approach see Blotter [2]. The remainder of this paper presents experimental results which validate the ESPF method.

2. EXPERIMENTAL SETUP

The ESPF approach was applied to a 380 mm x 300 mm x 1.6 mm steel plate. The plate had a Young's modulus of elasticity of 2.04E11 Pa, structural damping factor of 0.001, and Poisson's ratio of 0.29. The test plate was mounted to a rigid steel frame by thin steel shims as shown by Fig. 1. Five screws equally spaced along each edge of the plate were used to attach the plate to the shims. The test structure was designed to simulate a simply supported plate. However, this assumption is not made or required in any part of this experimental procedure, as the boundary conditions are inherently modeled in the solution based on the laser data.

The steel plate was harmonically excited with two electromagnetic shakers. The shakers were hung from bungee cords and connected to impedance heads. The impedance heads were connected to the plate through 2.0 cm diameter mount plates which were glued to the plate. Shaker 1, was attached to the plate at x=290 mm, y=90 mm. Shaker 2 was attached at x=90 mm, y=210 mm.

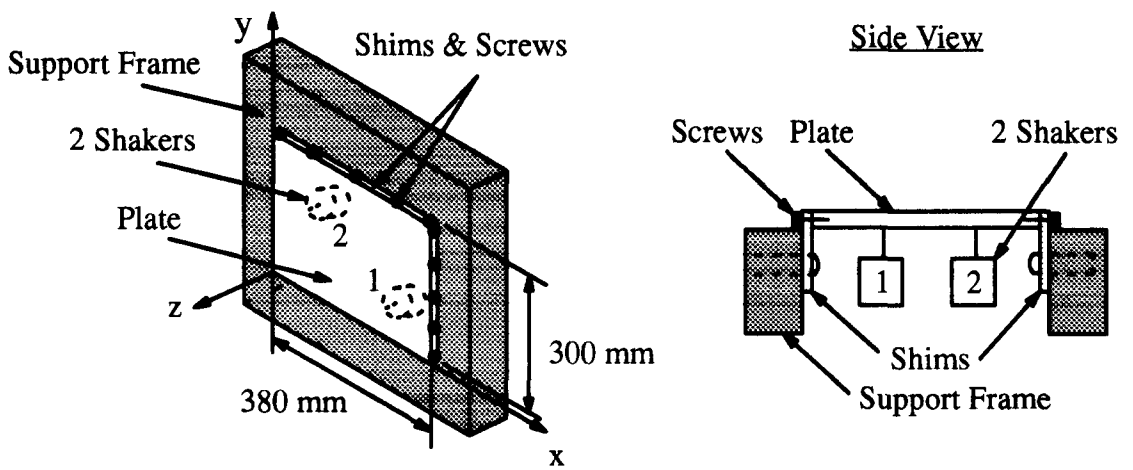

Figure 1. Simply supported plate experimental setup.

3. TEST PROCEDURE

Three methods of computing the power in the plate were compared to validate the ability of the ESPF method to conserve energy and provide qualitative power results. Method 1 consisted of using the ESPF method. Method 2 consisted of computing the power injected into the plate through the two shakers by collecting force and acceleration measurements from the two impedance heads during the scanning process. Method 3 consisted of computing the power injected into the plate through the two shakers by computing the cross spectrum of the force and acceleration signals from the impedance heads as shown by Eq. (1)[3].

$$P_{injected\ Method3} = \frac{\mathrm{Im}\{G_{fa}\}}{\omega} \tag{1}$$

In Eq. (1), ω is the forcing frequency, and $\mathrm{Im}\{G_{fa}\}$ is the imaginary component of the cross spectrum of the force and acceleration. Methods 2 and 3 produce identical results if the input signals are identical. However, in this setup, the signals in Method 2 are filtered and sampled using an A/D converter and a Silicon Graphics workstation. In Method 3, the signals are unfiltered and recorded by an HP 35665A Dynamic Signal Analyzer. The data used in Method 3 were collected after the scanning process was performed to show repeatability of the experiment. Since the two data acquisition methods are completely independent and the data were collected at slightly different times it should be realized that slight differences in the results will occur. By comparing the power results, the three methods can be used to validate each other.

4. EXPERIMENTAL RESULTS

The three power computation methods described in Section 3 were applied to the simply supported plate described in Section 2. The power flow results at forcing frequencies of 79.0 Hz and 909.0 Hz will be presented and discussed in this Section. Model order convergence effects for each frequency will also be discussed.

4.1. 79.0 HZ CASE

In the 79.0 Hz case the two shakers were phased such that shaker 2, as indicated in Fig. 1, lagged shaker 1 by 174.6 degrees and had a magnitude of 89% of shaker 1. These values were determined by plotting the magnitude and phase of the frequency response of the two input signals (output voltages leaving the signal generator into the power amplifier). The input signals were tuned such that the shakers had a relative phase slightly off of 180 degrees to ensure that a significant amount of active power in the plate would exist [4]. The plate was scanned from 5 different positions for a total of 32,000 points which were used to solve for the velocity field. The maximum velocity magnitude was 0.115 m/s. Using an 8x8 quintic B-spline mesh the mean and standard deviation of the residuals were 2.232E–04 and 1.751E–04 respectively. It was also noted that the residuals had a random distribution.

The vector plot shown in Fig. 2 illustrates the power flow in the plate as computed by the ESPF method. The magnitude of the velocity field indicating the operating shape of the plate is also superimposed on the power-flow vector plot. The darker areas of the velocity field representation indicate points of higher velocity. The 2 large black dots on the plate represent the

relative size and location of the shaker and impedance head mount plates while the small black dots on the plate boundaries represent the screw locations as discussed in Section 2.

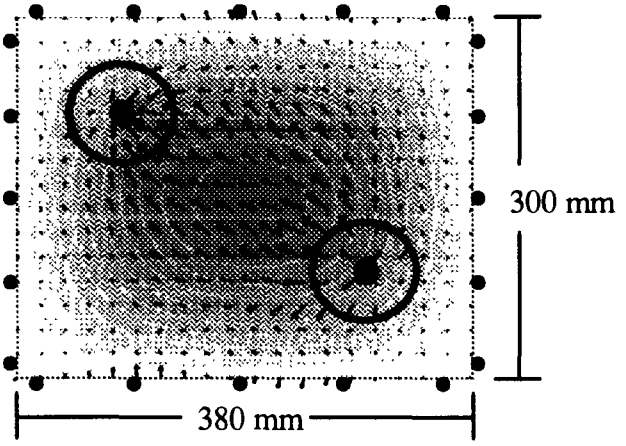

Figure 2. Power-flow vector plot and velocity field at 79.0 Hz

Figure 2 clearly indicates that under these conditions shaker 1 acts as a power source and shaker 2 acts as a power sink, and the main flow of power is in a direct path from shaker 1 to shaker 2. The large power flow vectors on the top and bottom of the plate are primarily due to two reasons. The first is that the simply supported plate conditions are not perfect in this experimental case and that indeed the bending moments are not exactly zero. The second reason is due to the effects of taking derivative of experimental data which magnifies any noise in the model. Even though the derivatives of the B-spline basis functions are used to compute the generalized forces instead of a finite difference approach some error propagates through these calculations. However, the problem of noise on the boundary can be reduced by tripling up the knots on the boundary in the B-spline mesh.

In experimental testing, true point forces can only be approximated. In this case, with the 2.0 cm diameter impedance head mount plates, point force conditions are not assumed or expected. Under ideal conditions with a 2.0 cm diameter mount plate the maximum power should occur at a radius of 1.0 cm from the center of the mount plate. Figure 2 indicates that the largest vectors are shown to occur slightly further than 1.0 cm away from the center of the mount plates. The large black ring surrounding the mount plate in Fig. 2 represents the circular control volume where the largest power in the plate is computed.

To further investigate this concern, the net power crossing a circular control volume, centered at the source, was computed. The control volume was then incrementally enlarged in the radial direction and the net power was again computed. The net power normal to each circular control volume was computed at 72 equally spaced points around each control volume. These 72 points were then used to compute the total power normal to the control volume. The total power in 30 control volumes at radial increments of 0.2 cm were computed for a total radial distance of 6.0 cm from the center of the mount plate. This same process was also performed for a set of control volumes centered at the sink.

Figures 3a and 3b show plots of the net power crossing each circular control volume for the 30 control volumes. Figure 3a illustrates that the maximum power of 0.17 W was obtained at a radial distance of 4.4 cm from the center of the source. This is 3.4 cm away from where the maximum power should theoretically occur. Figure 3b illustrates the decline in power as

it leaves through shaker 2. At a radial distance of 4.4 cm from the center of the sink a power value of –0.16 W was obtained.

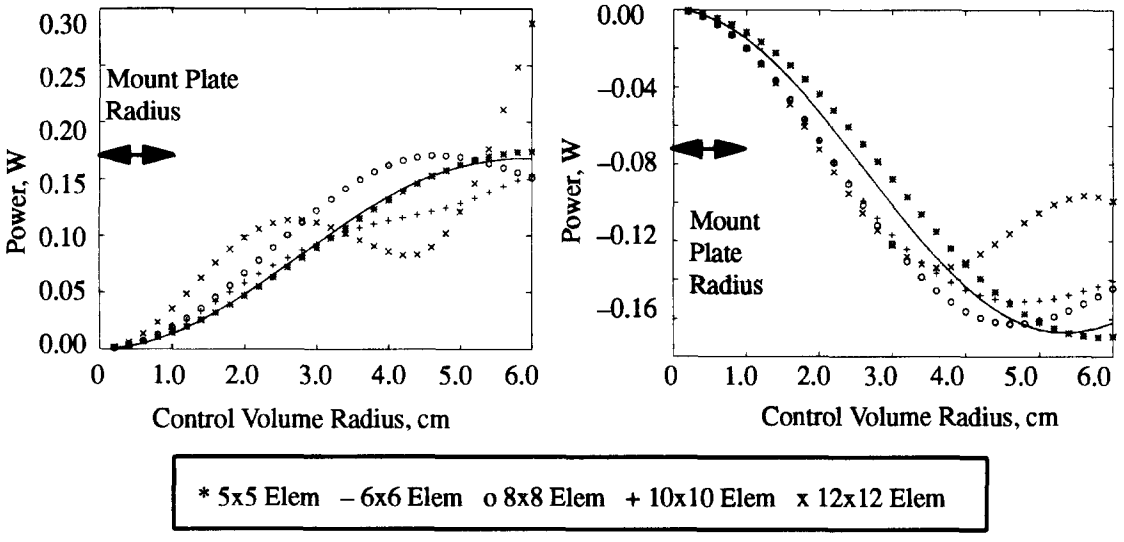

Figures 3a and 3b. Net power in each control volume around shaker 1 at 79.0 Hz

In Figs. 3a and 3b results from several mesh configurations are also shown. These results indicate that the model continues to converge through the 10x10 mesh and then over convergence is obtained. Over convergence is detected by the local maximum followed by an exponential increase in the power which represents and unrealistic situation.

To verify the maximum power values computed by the ESPF method, the control volume which contained the maximum power was compared to the injected power computations of Methods 2 and 3. It is expected that since the maximum power computed from the ESPF method does not occur exactly at the source that some difference between the comparison of the ESPF method and the injected power computations of Methods 2 and 3 will exist. It is further expected that the power values computed by the ESPF method will be slightly less than the power values computed by Methods 2 and 3 due to the losses in power which occur in the plate from the center of the source to the control volume where the ESPF computes the maximum power flow.

Table 1 summarizes these results and lists the percent difference between the three methods. The input power results computed from the three methods are as expected. The ESPF method predicts slightly less power than the power computed by Methods 2 and 3. The power leaving the system through shaker 2 does not follow this trend exactly. The power computed by the ESPF method is shown to fall between the power values computed by Methods 2 and 3. This slight difference is not of major concern due to the experimental errors which can effect the results.

Table 1. Comparison of the maximum power computed by the ESPF method and the injected power and absorbed power computed by Methods 2 and 3 at 79.0 Hz

Power Measurement Location and comparison definition	ESPF Method Max. Power in C. V. 8x8 mesh	Method 2 Z-Head using Iotech and SGI system	Method 3 Z-Head HP Analyzer cross spec. technique
Shaker 1 (source) W	+0.1706	+0.1908	+0.1845
Shaker 2 (sink) W	–0.1626	–0.1853	–0.1692
% diff. compared to Method 1 (gage 1, gage 2)	——— ———	+11.84 +3.96	+8.15 +4.06
% diff. compared to Method 2 (gage 1, gage 2)	–10.59 +12.25	——— ———	+3.30 +8.69
% diff. compared to Method 3 (gage 1, gage 2)	–7.53 –3.90	+3.41 –9.51	——— ———

4.2. 909.0 HZ CASE

The 909.0 Hz case is an off-resonance case. The purpose for showing this case is to illustrate the ability of the ESPF method to map the power-flow path at higher frequencies. The power flow map at 909.0 Hz is shown in Fig. 4a. This power-flow plot is much more complicated than the previous case where the power flow was shown to be in a direct flow path from the source to the sink. In this case, it appears as though the shakers act as both a source and sink. In the areas near the two shakers where large power vectors appear to dead end into each other is where significant acoustic radiation is generated.

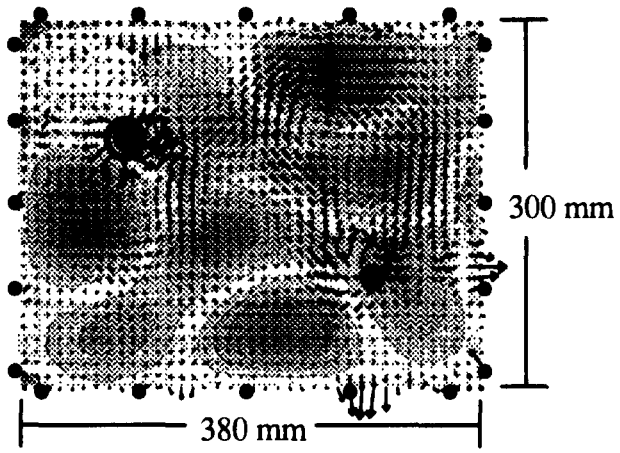

4a. Power flow vector plot at 909.0 Hz

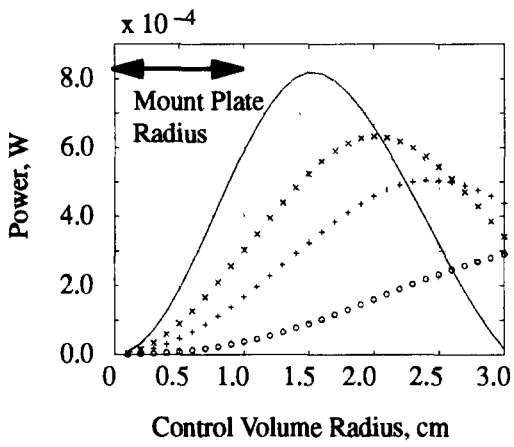

4b. Power in each control volume around shaker 2

o 8x8 Elem + 12x12 Elem x 15x15 Elem – 18x18 Elem . 20x20 Elem

Figures 4. Power flow 909.0 Hz

A similar convergence analysis was performed for the 909.0 Hz case as was performed for the 79.0 Hz case. Figure 4b shows that the model continues to converge both in magnitude and spatially up through the 18x18 element mesh. The 20x20 element mesh illustrates that the solution is starting to diverge and the resolving power in the model has become too great and noise in the model is beginning to be represented. The maximum power in the 18x18 element model is shown to occur at a radius of 1.5 cm from the center of the source. Given that the impedance head mount plates have a 1 cm radius it can be concluded that the maximum power was computed to within a radial distance of 0.5 cm. The circle surrounding shaker 2 in Fig. 4a represents the control volume where the maximum power was computed.

Table 2 summarizes the power magnitudes computed by all three methods. The maximum power values are shown in units of mW. The percent difference between these values are also listed in the table.

Table 2. Comparison of the maximum power computed by the ESPF method and the injected power and absorbed power computed by Methods 2 and 3 at 909.0 Hz

Power Measurement Location and comparison definition	ESPF Method Max. Power in C. V. 18x18 mesh	Method 2 Z-Head using Iotech and SGI system	Method 3 Z-Head HP Analyzer cross spec. technique
Shaker 2 (sink) mW	+0.817	+0.685	+0.665
% diff. compared to Method 1 (gage 2)	———	–16.16	–18.60
% diff. compared to Method 2 (gage 2)	+19.27	———	–2.91
% diff. compared to Method 3 (gage 2)	+22.86	+3.01	———

When performing the convergence analysis for the power around shaker 1 it was found that the results were extremely sensitive to the spatial location of the center of the control volumes. By reexamining Fig. 4a it is clearly evident that the location of the center of the control volumes around shaker 1 would have a large effect on the results due to the large power vectors which occur in all directions around the shaker. It can be understood that slight misplacement of the center of the control volumes could result in significant differences in the net power computed in each control volume. When comparing the power vectors surrounding shaker 1 and shaker 2, it is evident that shaker 2 appears much more like a regular source in that the power is projected in an outward direction all around the source. Around shaker 1 however, this does not occur.

5. SUMMARY

It was shown that the ESPF method predicted the magnitude of the input power to within approximately 10% of the power computed from impedance head measurements in the 79.0 Hz case. In the 909.0 Hz case the ESPF method predicted the power to within approximately 20% of the power computed from the impedance head measurements. The power flow results

also indicated that a spatial error of 4.4 cm was obtained when computing the exact location of the maximum power flow in the 79.0 Hz case. In the 311.0 Hz case the spatial error was 1.5 cm in predicting the location of the maximum power. Although the maximum power is computed slightly away from the source the location of the source and sink are still clearly identified by the power flow vector plots due to the symmetry of the excitation. The spatial error obtained in both these models could be reduced by localized mesh refinement capabilities. However, in most test conditions, when structures are large compared to the points of excitation or when the excitation is more of a distributed load this spatial error will be insignificant.

Although the ESPF method has many capabilities, the technique is currently limited to single frequency testing and transverse motion. Both broadband frequency testing and 3-D power flow capabilities are currently being pursued. Broadband testing will be performed by computing the FFT of the velocity signal from the laser at each scan point. The system will then be broken down into the main frequency components of interest and the velocity at each frequency will be solved for. The velocity field solver currently solves for the 3-D velocity field. However, the inplane velocity solution is extremely sensitive to the laser position and orientation which is determined using a laser registration algorithm [5]. Various methods to improve the laser registration have been investigated but a method to accurately extract the inplane velocities when they are near the noise floor of the laser has not been developed. To overcome this issue a complete error analysis of the entire ESPF process should be performed. This would identify the areas where noise contamination of the signals occurs and would possibly lead to a reduced noise floor which would enhance the quality of the inplane solution.

Further research in this area will also consist of improved calibration techniques, the implementation of non-uniform B-splines to allow local mesh refinement in the areas of concentrated loads, and the implementation of multiple knot configurations at the test specimen boundaries which will improve the derivative results at these locations.

REFERENCES

[1] G. Pavic, "Measurement of Structure Borne Wave Power Flow, Part 1: Formulation of the Methods," *Journal of Sound and Vibration* **49**, 1976, pp. 221-230.

[2] Blotter, J. D., "Structural Energy and Power Flow Using A Scanning Laser Doppler Vibrometer," *Ph.D. Dissertation*, Virginia Polytechnic Institute and State University, Blacksburg VA. 1996.

[3] J. W. Verheij, "Cross Spectral Density Methods for Measuring Structure Borne Power Flow on Beams and Pipes," *Journal of Sound and Vibration* **70**, 1980, pp. 133-139.

[4] N. Tanaka, S. D. Synder, Y. Kikushima, and M Kuroda, Vortex Structural Power Flow in a Thin Plate and the Influence on the Acoustic Field, *Journal of the Acoustical Society of America* **96**, 1994, pp. 1563-1574.

[5] Lindholm, B. E., 1996, "Three-Dimensional Position Registration for a Scanning Laser Doppler Vibrometer," *Proceedings of the 14th International Modal Analysis Conference*, pp. 830-836,